INDIAN JOURNAL OF SCIENCE AND TECHNOLOGY

RESEARCH ARTICLE

Muntz – Legendre Wavelet Operational Matrix Method to Compute a Numerical Solution for Thermal Radiation Effect on Natural Convection Boundary Layer Flow past a Vertical Plate Embedded in a Saturated Porous Medium

S C Shiralashetti[1]*, E Harishkumar[1], S I Hanaji[2]

1 Department of Mathematics, Karnatak University, Dharwad, 580003, Karnataka, India
2 Department of Mathematics, Dr. M. S. Sheshgiri College of Engineering and Technology, Belagavi, 590008, Karnataka, India

OPEN ACCESS

Received: 05-08-2022
Accepted: 04-11-2022
Published: 21-12-2022

Citation: Shiralashetti SC, Harishkumar E, Hanaji SI (2022) **Muntz – Legendre** Wavelet Operational Matrix Method to Compute a Numerical Solution for Thermal Radiation Effect on Natural Convection Boundary Layer Flow past a Vertical Plate Embedded in a Saturated Porous Medium. Indian Journal of Science and Technology 15(48): 2777-2790. https://doi.org/10.17485/IJST/v15i48.1619

* **Corresponding author**.

scshiralashetti@kud.ac.in

Funding: UGC-SAP DRS-III for 2016-2021:F.510/3/DRS-III / 2016(SAP-I). Karnatak University, Dharwad (KUD), Karnataka, India through a University Research Studentship (URS) during the year 2018-2021: KU.40 (SC/ST) sch/URS/2020-21/44/544, dated 12/12/2020

Competing Interests: None

Published By Indian Society for Education and Environment (iSee)

ISSN
Print: 0974-6846
Electronic: 0974-5645

Abstract

Objectives: In this present framework, heat transfer of the thermal radiation effect on natural convection around a vertical permeable flat surface immersed in a saturated porous medium has been investigated by considering the thermal radiation effect. **Methods**:The governing partial differential equations of the considered problem are converted to the nonlinear ordinary differential equations over the infinite domain with the aid of similarity transformations. In order to analyze the thermal radiation, the Müntz – Legendre wavelet operational matrix method has been considered to solve the corresponding nonlinear ordinary differential equation. **Findings**:To check the efficiency of the proposed strategy, the third-order nonlinear boundary value problem having the exact solution is considered a test problem. Also, the obtained findings are compared with the findings of the Haar wavelet operational matrix method. **Novelty**: The three physical parameters of temperature exponent λ thermal radiation R_d, and Injection/suction f_m on vertical velocity and temperature profiles are demonstrated and discussed graphically. Also, the comparison of the Müntz – Legendre wavelet operational matrix method results with Haar wavelet operational matrix method results ensure that the solutions obtained by Müntz – Haar wavelet operational matrix method results.

Keywords: Muntz-legendre wavelet; Operational matrix; Natural convection; Thermal radiation; Saturated porous medium; Suction/Injection

1 Introduction

Heat transfer in convection saturated porous medium have been initiated increasing interest in studying their significance in many applications in geophysical and

engineering such as thermal insulation, drying of porous solids, geothermal reservoirs, enhanced oil recovery, cooling of nuclear reactors, packed-bed catalytic reactors, under ground energy transport, etc.[1]. The study of heat transfer in a free convective vertical flat plate immersed in a porous medium with an internal heat generation problem is solved by Cortell R with the aid of the Fourth-order Runge-Kutta algorithm[2]. This work is extended on the previous work of the authors Driss Achemlal et al. who have investigated the effect of heat source and thermal radiation flux around a vertical plate immersed in a porous medium by using the fifth-order Runge-Kutta scheme associated with the shooting technique[3]. And also the authors Talha Anwar et al. have analyzed the effect of thermal radiation on convective heat transfer across a porous moving vertical plate[4]. The authors Nourhan et al. have studied the influence of wall heat flux on the thermal radiation on natural convection fluid flow along a vertical cone immersed in a saturated porous media[5]. Recently, many researchers have seemed regarding the interplay of vertical plates immersed in a saturated porous medium with convection flows by solving the numerical techniques. The authors Mahdy et al. and Jha B K et al. have studied the effect of the presence or absence of internal heat generation and thermal radiation[6–8]. The authors Roja P et al. and Jha B K et al. have investigated some related porous medium cases with thermal radiation and also discussed velocity and temperature profiles[9,10]. Our proposed third-order nonlinear problem with corresponding boundary conditions is numerically solved by using a newly modified Müntz – Legendre wavelet operational matrix method (MLWOMM). Because we selected problems that are not applied to wavelet-based numerical methods. So we concentrate on those nonlinear problems to solve them by applying MLWOMM. It obtained good results and more accurate solutions.

In recent years, MLWOMM is one of the most widely used wavelet methods for calculating numerical results in differential equations. Nowadays, many researchers have discussed applying numerical techniques to find the results of nonlinear ordinary differential equations (ODEs). In the last few decades, various numerical techniques have been introduced, to name a few, the Shooting method, Finite difference method, Keller box method, Haar wavelet method, etc., these numerical methods are computing the results of boundary value problems (BVPs). MLWOMM is the more effective method for solving the BVPs with finite intervals. Recent research articles are available on various types of wavelets techniques for computing linear and nonlinear differential equations with finite domains, to name a few, Haar wavelet method[11,12], Daubechies wavelet method[13], Fibonacci wavelet method[14], Chebyshev wavelet method[15], Hermite wavelet method[16], Legendre wavelet method[17], etc. Alfred Haar is the first one who introduced the notation of wavelets in the year 1909 and this work is extended by Grossmann and Morlet[18]. The authors Shiralashetti et al. have investigated finding the numerical solution of the strategy of wavelet operational matrix in great detail and used it in differential equations[19,20]. Authors Karkera et al. have briefly investigated the numerical solution of third-order boundary layer Magnetohydrodynamics flow due to stretching sheet by applying the Haar wavelet collocation method (HWCM)[21]. Furthermore, V. B. Awati et al. discussed the forced convection of third-order boundary layer flow problems that are solved in the Haar wavelet technique[22]. Recently, many authors have investigated different problems in differential equations and solving on the MLWOMM and they have detailed discussed calculating the Müntz – Legendre wavelet operational matrix procedure[23–25]. This technique is very precise and satisfactory compare to the Haar wavelet results.

The main goal of this article is to investigate the heat transfer problem on the effect of thermal radiation presence in a saturated porous medium. First, to check the efficiency of the MLWOMM solution by implementing it on the boundary value problem and comparing it with the Haar wavelet results with the exact solutions; it gives accurate results compared to the Haar wavelet operational matrix method (HWOMM) results. So we have utilized the MLWOMM to solve the thermal radiation problem and compare it with the velocity or temperature profiles of HWOMM results, and also investigated on effects of thermal radiation with fluid suction/injection. The effects of several selected parameters such as R_d, f_m and λ, have been discussed in detail and presented in terms of graphs and tables.

2 Methodology

2.1 Mathematical preliminaries of Müntz-Legendre wavelets

Wavelets have been employed with great success in a variety of scientific and technical domains. A family of functions is constructed by mother wavelets from dilating and translating themselves into a single function, which we call mother wavelets. The family of continuous wavelets is following[14]:

$$\psi_{a,b}(\eta) = |a|^{-\frac{1}{2}} \psi\left(\frac{\eta - b}{a}\right), \quad a, b \in R, a \neq 0.$$

Where, a is the dilation b is the translation parameter, Nevertheless, the translation parameter b varies continuously. Similarly, a and b are the parameters of discrete values as $a = a_0^{-k}, b = nb_0a_0^{-k}, a_0 > 1, b_0 > 0$.

Where $n,k \in N$ we have the following family of discrete wavelets may be given as

$$\psi_{n,k}(\eta) = |a|^{-\frac{k}{2}} \psi\left(a_0^k \eta - nb_0\right), \quad a,b \in R, a \neq 0.$$

Where, $\psi_{n,k}$ are the wavelet bases in $L^2(R)$. Furthermore, $a = 2,$ and $b = 1$then form the orthonormal basis $\psi_{n,k}(\eta)$.

2.1.1 Müntz-Legendre polynomials

The polynomials of the n^{th}Müntz – Legendre which are defined on the interval by$[0,1)$ [25], we have

$$L_m(\eta) = \sum_{k=0}^{m} \xi_{k,m} \eta^{\lambda k}, \quad \xi_{0,0} = 1, \quad \xi_{k,m} = \frac{\prod_{j=0}^{m-1}(\lambda_k + \lambda_j + 1)}{\prod_{j=0, j\neq k}^{m}(\lambda_k - \lambda_j)}, m \in N_0.$$

The satisfy orthogonality criteria for these polynomials are as follows

$$\int_0^1 L_n(\eta) L_m(\eta) d\eta = \left(\frac{\delta_{n,m}}{2\lambda_m + 1}\right), \quad (m \geq n).$$

Here, $\delta_{n,m}$ is defined as the Kronecker symbol. And also the also the Müntz – Legendre polynomials have been satisfied in terms of recursive formula:

$$L_m(\eta) = L_{m-1}(\eta) - (\lambda_m + \lambda_{m-1} + 1)\eta^{\lambda_m} \int_\eta^1 \eta^{-\lambda_m - 1} L_{m-1}(\eta) d\eta, \quad \eta \in (0,1).$$

In this research article, we assume that $\lambda_k = k\gamma$. Here γ is a real constant. In general, the Müntz – Legendre polynomials have been described in terms of recurrence relation as [25] :

$$L_m(\eta) = \sum_{k=0}^{m} \xi_{k,m} \eta^{\lambda k}, \quad \xi_{0,0} = 1, \quad \xi_{k,m} = \frac{(-1)^{m-k}}{\gamma^m k!(m-k)!} \prod_{z=0}^{m-1}((k+z) \times \gamma + 1). \tag{1}$$

Where, $k = 0,1,2,\ldots,m,$ and $L_m(\eta)$ are the Müntz – Legendre polynomials of the order $m$in the finite intervals $\eta \in [0,1)$, generally, we can define the first few polynomials for$\lambda_k = k\gamma, \gamma = 1/2$ are

$$\left.\begin{aligned}
&L_0(\eta) = 1,\\
&L_1(\eta) = 3\eta^{1/2} - 2,\\
&L_2(\eta) = 10\eta - 12\eta^{1/2} + 3,\\
&L_3(\eta) = 30\eta^{1/2} - 60\eta + 35\eta^{3/2} - 4,\\
&L_4(\eta) = 210\eta + 126\eta^2 - 60\eta^{1/2} - 280\eta^{3/2} + 5,\\
&L_5(\eta) = 105\eta^{1/2} - 1260\eta^2 - 560\eta + 1260\eta^{3/2} + 462\eta^{5/2} - 6,\\
&L_6(\eta) = 1260\eta + 6930\eta^2 - 168\eta^{1/2} + 1716\eta^3 - 4200\eta^{3/2} - 5544\eta^{5/2} + 7,\\
&L_7(\eta) = 252\eta^{1/2} - 27720\eta^2 - 2520\eta - 24024\eta^3 + 11550\eta^{3/2} + 36036\eta^{5/2} + 6435\eta^{7/2} - 8,
\end{aligned}\right\}. \tag{2}$$

2.1.2 Müntz-Legendre wavelets and Function approximation

Müntz – Legendre wavelets are a type of compactly supported wavelet formed by Müntz – Legendre polynomials over the interval $[-1,1]$. Generally, the Müntz – Legendrewavelets can be represented as in the interval, $[0,1)$, we have [25] :

$$\psi_{n,m}(\eta) = \begin{cases} \sqrt{(2\lambda_m + 1)} 2^{\frac{k-1}{2}} L_m\left(2^{k-1}\eta - \hat{n}\right), & \left(\frac{n-1}{2^{k-1}} \leq \eta < \frac{n}{2^{k-1}}\right), \\ 0, & \text{otherwise.} \end{cases} \tag{3}$$

The Müntz – Legendre wavelets have introduced by $\psi_{n,m}(\eta) = \psi(\hat{n},k,m,\eta)$, here they are 4-arguments, where, $\hat{n} = n - 1, n = 1,2,3,4,\ldots,2^{k-1}$ assume that $k$is any positive numbers η represented the time and m can be considered the order of Müntz – Legendre polynomials. Where, k and $n$represent the level of resolution with translation parameter, and $L_m(\eta)$ is the Müntz – Legendre polynomial of degree m. With $m = 0,1,2,\ldots,M-1$and the coefficients of $\sqrt{(2\lambda_m + 1)}$ is orthonormality,

if the dilation and translation parameters $a = 2^{-k}, b = \hat{n}2^{-k}$. The Müntz – Legendre wavelets $\psi_{n,m}(\eta)$are also formed orthonormality concerning weight function $w(\eta) = 1$.

The Müntz – Legendre wavelets in Eq. (3) are also represented in the following way:

$$\psi_{n,m}(\eta) = \sqrt{(2\lambda_m + 1)}2^{\frac{k-1}{2}} L_m\left(2^{k-1}\eta - n + 1\right)\chi_{I_{n,k}}(\eta), \tag{4}$$

Where $\chi_{I_{n,k}}(\eta)$ is the specified characteristic function on $\left[\frac{n-1}{2^{k-1}}, \frac{n}{2^{k-1}}\right]$, for the instance, we choose $k = 2, M = 4,$ and $\gamma = 1/2$. The eight bases of the Müntz – Legendrewavelet family, we have:

$$\left.\begin{array}{l}
\left.\begin{array}{l}
\psi_{1,0}(\eta) = \sqrt{2}\,, \\
\psi_{1,1}(\eta) = \sqrt{4}\left(3(2\eta)^{1/2} - 2\right), \\
\psi_{1,2}(\eta) = \sqrt{6}\left[10(2\eta) - 12(2\eta)^{1/2} + 3\right], \\
\psi_{1,3}(\eta) = \sqrt{8}\left[30(2\eta)^{1/2} - 60(2\eta) + 35(2\eta)^{3/2} - 4\right],
\end{array}\right\}, \quad 0 \le \eta < \frac{1}{2}, \\
\left.\begin{array}{l}
\psi_{2,0}(\eta) = \sqrt{2}\,, \\
\psi_{2,1}(\eta) = \sqrt{4}\left(3(2\eta - 1)^{1/2} - 2\right), \\
\psi_{2,2}(\eta) = \sqrt{6}\left[10\,(2\eta - 1) - 12(2\eta - 1)^{1/2} + 3\right], \\
\psi_{2,3}(\eta) = \sqrt{8}\left[30(2\eta - 1)^{1/2} - 60(2\eta - 1) + 35(2\eta - 1)^{3/2} - 4\right],
\end{array}\right\}, \quad \frac{1}{2} \le \eta < 1,
\end{array}\right\}. \tag{5}$$

The Müntz – Legendre wavelets may be used to extend any square-integrable function that can be defined on $f(\eta) \in L^2[0,1)$. we have,

$$f(\eta) = \sum_{n=1}^{\infty}\sum_{m=0}^{\infty} a_{n,m}\psi_{n,m}(\eta). \tag{6}$$

By truncating the above infinite series, we have

$$f(\eta) = \sum_{n=1}^{2^{k-1}}\sum_{m=0}^{M-1} a_{n,m}\psi_{n,m}(\eta) = a^T\Phi(\eta). \tag{7}$$

Where,

$$a_{n,m} = \langle f(\eta), \psi_{n,m}(\eta)\rangle = \int_0^1 f(\eta)\psi_{n,m}(\eta)d\eta, \tag{8}$$

Eq. (10) represents unknown coefficients of the Müntz – Legendre wavelet, and also the matrix equivalent of Eq. (11) is as follows[25]:

$$f(\eta) = a^T\Phi(\eta), \tag{9}$$

where, $a$is a form of row vector-that can be written as

$$a = \left[a_{1,0}, a_{1,1}, a_{1,2}, \ldots, a_{1,M-1}, a_{2,0}, a_{2,1}, \ldots, a_{2,M-1}, \ldots, a_{2^{\star-1},0}, a_{2^{\star-1},1}, \ldots, a_{2^{\star-1},M-1}\right]^T, \tag{10}$$

and the matrix $\Phi(\eta)$ is $\left(2^{k-1}M \times 1\right)$

$$\Phi(\eta) = \left[\psi_{1,0}(\eta), \psi_{1,1}(\eta), \psi_{1,2}(\eta), \ldots, \psi_{1,M-1}(\eta), \psi_{2,0}(\eta), \psi_{2,1}(\eta), \ldots, \psi_{2,M-1}(\eta), \ldots, \psi_{2^{k-1},0}(\eta), \psi_{2^{k-1},1}(\eta), \ldots, \psi_{2^{k-1},M-1}(\eta)\right]^T. \tag{11}$$

By using suitable collocation points are as follows:

$$\eta_l = \frac{(2l-1)}{2^k M}, l = 1, 2, \ldots, 2^{k-1}M. \tag{12}$$

For instance, if $k=2$ and $M=4$ we can write matrix form

$$\Phi_{8\times 8}=\begin{pmatrix} 1.4142 & 1.4142 & 1.4142 & 1.4142 & 0 & 0 & 0 & 0 \\ -1.8787 & -0.3258 & 0.7434 & 1.6125 & 0 & 0 & 0 & 0 \\ 0.0180 & -1.4659 & -0.5801 & 1.2861 & 0 & 0 & 0 & 0 \\ 1.8481 & -0.2586 & -1.3837 & 0.5925 & 0 & 0 & 0 & 0 \\ 0 & 0 & 0 & 0 & 1.4142 & 1.4142 & 1.4142 & 1.4142 \\ 0 & 0 & 0 & 0 & -1.8787 & -0.3258 & 0.7434 & 1.6125 \\ 0 & 0 & 0 & 0 & 0.0180 & -1.4659 & -0.5801 & 1.2861 \\ 0 & 0 & 0 & 0 & 1.8481 & -0.2586 & -1.3837 & 0.5925 \end{pmatrix}. \tag{13}$$

2.1.3 Operational matrix of Müntz-Legendre wavelets

In the present section, we construct the operational matrices of Müntz – Legendre wavelets. The authors Shiralashetti et al. have introduced the strategy of operational matrices of integration [20], we have:

$$\int_0^\eta \Phi(\eta)d\eta = P\Phi(\eta). \tag{14}$$

Where, P is the order of $2^{k-1}M\times 2^{k-1}M$Müntz – Legendrewavelet operational matrix. Now we have illustrated the procedure of calculating the Müntz – Legendre operational coefficient matrix P. In particular, if $k=2, M=4$ and $\gamma=1/2$. Firstly, we can choose eight basis functions that are represented in Eq. (5), by integrating Eq. (5) by using corresponding collocation points provided in Eq. (12) we will get

$$\int_0^\eta \psi_{1,0}(\eta)d\eta=\begin{cases}\sqrt{2}\eta, & \eta\in\left[0,\frac{1}{2}\right)\\ \frac{\sqrt{2}}{2}, & \eta\in\left[\frac{1}{2},1\right)\end{cases}=\left[\tfrac{1}{4},\ \tfrac{197}{1393},\ \tfrac{14}{485},\ 0,\ \tfrac{1}{2},\ 0,\ 0,\ 0\right]^T\Phi_8(\eta)\ ,$$

$$\int_0^\eta \psi_{1,1}(\eta)d\eta=\begin{cases}4\sqrt{2}\eta^{3/2}-4\eta, & \eta\in\left[0,\frac{1}{2}\right)\\ 0, & \eta\in\left[\frac{1}{2},1\right)\end{cases}=\left[-\tfrac{197}{1393},\ 0,\ \tfrac{41}{703},\ \tfrac{2}{99},\ 0,\ 0,\ 0,\ 0\right]^T\Phi_8(\eta),$$

$$\int_0^\eta \psi_{1,2}(\eta)d\eta=\begin{cases}\sqrt{6}\eta\left(10\eta-8\times 2^{1/2}\eta^{1/2}+3\right), & \eta\in\left[0,\frac{1}{2}\right)\\ 0, & \eta\in\left[\frac{1}{2},1\right)\end{cases}=\left[-\tfrac{26}{625},-\tfrac{29}{962},-\tfrac{7}{185},\tfrac{41}{607},0,0,0,0\right]^T\Phi_8(\eta),$$

$$\int_0^\eta \psi_{1,3}(\eta)d\eta=\begin{cases}-8\eta\left(15\times 2^{1/2}\eta+2^{1/2}-10\eta^{1/2}-14\eta^{3/2}\right), & \eta\in\left[0,\frac{1}{2}\right)\\ 0, & \eta\in\left[\frac{1}{2},1\right)\end{cases}=\left[-\tfrac{1}{31},\tfrac{11}{284},\ -\tfrac{85}{691},\tfrac{59}{1041},\ 0,0,0,0\right]^T\Phi_8(\eta)\ ,$$

$$\int_0^\eta \psi_{2,0}(\eta)d\eta=\begin{cases}0, & \eta\in\left[0,\frac{1}{2}\right)\\ \sqrt{2}\left(\eta-\frac{1}{2}\right), & \eta\in\left[\frac{1}{2},1\right)\end{cases}=\left[0,\ 0,\ 0,\ 0,\ \tfrac{1}{4},\ \tfrac{197}{1393},\ \tfrac{14}{485},\ 0\right]^T\Phi_8(\eta),$$

$$\int_0^\eta \psi_{2,1}(\eta)d\eta=\begin{cases}0, & \eta\in\left[0,\frac{1}{2}\right)\\ 2(2\eta-1)^{3/2}-4\eta+2, & \eta\in\left[\frac{1}{2},1\right)\end{cases}$$

$$=\left[0,\ 0,\ 0,\ 0,\ -\tfrac{197}{1393},\ 0,\ \tfrac{41}{703},\ \tfrac{2}{99}\right]^T\Phi_8(\eta),$$

$$\int_0^\eta \psi_{2,2}(\eta)d\eta=\begin{cases}0, & \eta\in\left[0,\frac{1}{2}\right)\\ \sqrt{6}\left(7\eta+4(2\eta-1)^{3/2}-10\eta^2-1\right), & \eta\in\left[\frac{1}{2},1\right)\end{cases}$$

$$=\left[0,0,\ \ 0,0,-\tfrac{26}{625},-\tfrac{29}{962},-\tfrac{7}{185},\tfrac{41}{607}\right]^T\Phi_8(\eta),$$

$$\int_0^\eta \psi_{2,3}(\eta)d\eta=\begin{cases}0, & \eta\in\left[0,\frac{1}{2}\right)\\ 112\sqrt{2}\eta+20\sqrt{2}(2\eta-1)^{3/2}+14\sqrt{2}(2\eta-1)^{5/2}-26\sqrt{2}-120\sqrt{2}\eta^2, & \eta\in\left[\frac{1}{2},1\right)\end{cases}$$

$$=\left[0,\ \ 0,0,\ \ 0,-\tfrac{1}{35},\tfrac{11}{284},\ \ -\tfrac{85}{691},\tfrac{59}{1041}\right]^T\Phi_8(\eta).$$

Therefore, in the following Eq. (15), we obtain the form:

$$\int_0^\eta \Phi_{8\times 1}(\eta)d\eta = P_{8\times 8}\Phi_8(z), \tag{15}$$

where,

$$P_{8\times 8}=\begin{pmatrix} 0.2500 & 0.1414 & 0.0289 & 0 & 0.5000 & 0 & 0 & 0 \\ -0.1414 & 0 & 0.0583 & 0.0202 & 0 & 0 & 0 & 0 \\ -0.0416 & -0.0301 & -0.0378 & 0.0675 & 0 & 0 & 0 & 0 \\ -0.0286 & 0.0387 & -0.1230 & 0.0567 & 0 & 0 & 0 & 0 \\ 0 & 0 & 0 & 0 & 0.2500 & 0.1414 & 0.0289 & 0 \\ 0 & 0 & 0 & 0 & -0.1414 & 0 & 0.0583 & 0.0202 \\ 0 & 0 & 0 & 0 & -0.0416 & -0.0301 & -0.0378 & 0.0675 \\ 0 & 0 & 0 & 0 & -0.0286 & 0.0387 & -0.1230 & 0.0567 \end{pmatrix}. \tag{16}$$

Similarly, we maintain the same procedure, integrating Eq. (15) we will find that Q and R are the operational matrices. We have

$$\int_0^\eta \int_0^\eta \Phi(\eta)d\eta d\eta = Q_{8\times 8}\Phi_8(\eta), \tag{17}$$

$$\int_0^\eta \int_0^\eta \int_0^\eta \Phi(\eta)d\eta d\eta d\eta = R_{8\times 8}\Phi_8(\eta), \tag{18}$$

where,

$$Q_{8\times 8} = \begin{pmatrix} 0.0413 & 0.0345 & 0.0144 & 0.0048 & 0.2500 & 0.0707 & 0.0144 & 0 \\ -0.0384 & -0.0210 & -0.0088 & 0.0051 & -0.0707 & 0 & 0 & 0 \\ -0.0001 & -0.0029 & -0.0092 & 0.0002 & -0.0144 & 0 & 0 & 0 \\ 0.0050 & -0.0009 & 0.0015 & -0.0062 & 0 & 0 & 0 & 0 \\ 0 & 0 & 0 & 0 & 0.0413 & 0.0345 & 0.0144 & 0.0048 \\ 0 & 0 & 0 & 0 & -0.0384 & -0.0210 & -0.0088 & 0.0051 \\ 0 & 0 & 0 & 0 & -0.0001 & -0.0029 & -0.0092 & 0.0002 \\ 0 & 0 & 0 & 0 & 0.0050 & -0.0009 & 0.0015 & -0.0062 \end{pmatrix}, \tag{19}$$

$$R_{8\times 8} = \begin{pmatrix} 0.0049 & 0.0056 & 0.0021 & 0.0019 & 0.0727 & 0.0349 & 0.0108 & 0.0024 \\ -0.0057 & -0.0051 & -0.0025 & -0.0008 & -0.0362 & -0.0100 & -0.0020 & 0 \\ 0.0013 & 0.0001 & 0.0003 & -0.0008 & -0.0031 & -0.0020 & -0.0004 & 0 \\ 0.0009 & 0.0004 & 0.0008 & -0.0003 & 0.0020 & 0 & 0 & 0 \\ 0 & 0 & 0 & 0 & 0.0049 & 0.0056 & 0.0021 & 0.0019 \\ 0 & 0 & 0 & 0 & -0.0057 & -0.0051 & -0.0025 & -0.0008 \\ 0 & 0 & 0 & 0 & 0.0013 & 0.0001 & 0.0003 & -0.0008 \\ 0 & 0 & 0 & 0 & 0.0009 & 0.0004 & 0.0008 & -0.0003 \end{pmatrix}. \tag{20}$$

2.2 Müntz-Legendre wavelet operational matrix method of solution

In this section, we developed a numerical solution to a nonlinear third-order Boundary value problem and heat transfer problem on natural convection about a vertical plate immersed in a saturated porous medium arising in heat and mass transfer. For the test applicability of the Müntz – Legendre wavelets, we concentrate on the following boundary value problems that are defined with the intervals on $[0,1)$. And we consider the general form of the third-order differential equation as follows:

$$F'''(\eta) = f\left(\eta, F, F', F''\right). \tag{21}$$

Following Shiralashetti et al.[17], we assume that

$$F'''(\eta) = \sum_{l=1}^{2^{k-1}M} a_l \psi(\eta) = a^T \Phi(\eta), \tag{22}$$

where, a^T is the unknown Müntz – Legendre wavelet coefficients and integrating the above Eq. (22) from 0 to η, we have

$$F''(\eta) = F''(0) + \sum_{l=1}^{2^{k-1}M} a_i P(\eta) = F''(0) + a^T P(\eta), \tag{23}$$

integrating the above Eq. (23) from 0 to η, we have:

$$F'(\eta) = F'(0) + \eta F''(0) + \sum_{l=1}^{2^{k-1}M} a_i Q(\eta) = F'(0) + \eta F''(0) + a^T Q(\eta), \tag{24}$$

again integrating the above Eq. (24) from 0 to η, we get $F(\eta)$

$$F(\eta) = F(0) + \eta F'(0) + \frac{\eta^2}{2}F''(0) + \sum_{l=1}^{2^{k-1}M} a_l R(\eta) = F(0) + \eta F'(0) + \frac{\eta^2}{2}F''(0) + a^T R(\eta). \tag{25}$$

In the above Eq. (25) we find $F''(0)$ using boundary conditions and if we set $\eta_\infty = 1$, we get

$$F''(0) = \left[F'(1) - F'(0) - \sum_{i=1}^{2^{k-1}M} a_l E_l\right] = \left[F'(1) - F'(0) - a^T E\right]. \tag{26}$$

Here, $E = \int_0^1 P_l(\eta)d\eta$. Now we have substituted the values $F(\eta), F'(\eta), F''(\eta), F'''(\eta)$ and $f''(0)$ in Eq. (21) and applied them using collocation points given in Eq. (12), finally, a $2^{k-1}M \times 2^{k-1}M$ nonlinear system is obtained. To solve a nonlinear system to calculate the unknowns of M*ü* ntz-Legendre wavelet coefficients $a_i'S$ Newton's iterative technique is applied. The received $a_i'S$ values are substituted in the Eq. (25), and we get the MLWOMM solution.

2.3 Müntz-Legendre wavelet operational matrix method of implementation

In this section, we developed a numerical solution for a system of third-order nonlinear boundary value problems and the effect of thermal radiation problem on the natural convection of vertical plate embedded in a saturated porous medium, by using the MLWOMM, in the interval $[0,1)$. The received results are compared with the Haar wavelet solutions.

Test problem 1. Firstly, we consider the third-order nonlinear boundary value problem [26]:

$$\left.\begin{array}{c} F'''(\eta)-\eta^4F(\eta)+[F(\eta)]^2-g(\eta)=0, \quad 0<\eta<1, \eta\in[0,1], \\ F(0)=0, F'(0)=-1, \quad F'(1)=\sin(1). \end{array}\right\}, \tag{27}$$

Here, $g(\eta)=-3\sin(\eta)-\cos(\eta)(\eta-1)-\eta^4(\eta-1)\sin(\eta)+(\eta-1)^2\sin^2(\eta)$.

Eq. (27) has the exact solution as $F(\eta)=(\eta-1)\sin(\eta)$.

Now we have substituted the values $F'''(\eta)$ and $F(\eta)$, in Eq. (27), from section 2.2 and applied them using collocation points given in Eq. (12), finally, a third-order nonlinear system is obtained.

$$a^T\left[\Phi(\eta)-\eta^4R(\eta)\right]-\frac{\eta^6}{2}\left[\sin(1)-a^TE+1\right]+\left[a^TR(\eta)-\eta+\frac{\eta^2}{2}\left[\sin(1)-a^TE+1\right]\right]^2+\eta^5-g(\eta)=0. \tag{28}$$

If $k=2, M=4 \Rightarrow 2^{k-1}\times M=8, \gamma=0.5, \quad \eta\in[0,1)$ for instance, we have the nonlinear system is obtained.

Solving the above nonlinear system to find the unknowns of Müntz – Legendre wavelet coefficients $a_l'S$ Newton's iterative technique is applied. We take $k=2$, $M=4$, and $\gamma=0.5$. The received calculated unknown Müntz – Legendre wavelet coefficients $a_1=-0.0082$, $a_2=-0.4006$, $a_3=-0.0829$, $a_4=0.0048$, $a_5=-1.2944$, $a_6=-0.3073$, $a_7=-0.0489$, $a_8=0.0132$, these values are substituted in Eq. (25), and we get the MLWOMM solution. The collected results are presented in terms of Table and graph. The effectiveness of MLWOMM is presented by comparison with exact solutions and HWOMM solutions which are demonstrated in Table 1. The obtained numerical results show in Figure 1. The displayed, Table and graph clearly show that the comparisons of MLWOMM solutions are in great agreement with the exact solutions, and more accurate solutions compare to HWOMM solutions.

Table 1. Comparison of MLWOMM, and HWOMM with exact solutions of Test problem 1.

For instance $k=2, M=8, \gamma=0.5$					
η	**Exact solution**	**HWOMM solution**	**MLWOMM solution**	**Absolute error**	**Absolute error**
0.0313	-0.0303	-0.0306	-0.0303	0.0003	0.0000
0.0938	-0.0848	-0.0870	-0.0848	0.0021	0.0000
0.1563	-0.1313	-0.1360	-0.1312	0.0047	0.0001
0.2188	-0.1695	-0.1768	-0.1694	0.0073	0.0001
0.2813	-0.1995	-0.2087	-0.1993	0.0092	0.0002
0.3438	-0.2212	-0.2313	-0.2209	0.0102	0.0003
0.4063	-0.2346	-0.2448	-0.2342	0.0102	0.0004
0.4688	-0.2400	-0.2494	-0.2395	0.0094	0.0005
0.5313	-0.2375	-0.2454	-0.2375	0.0080	0.0000
0.5938	-0.2273	-0.2335	-0.2273	0.0062	0.0000
0.6563	-0.2097	-0.2140	-0.2097	0.0043	0.0000
0.7188	-0.1852	-0.1878	-0.1852	0.0026	0.0000
0.7813	-0.1540	-0.1553	-0.1540	0.0012	0.0000
0.8438	-0.1167	-0.1171	-0.1167	0.0004	0.0000
0.9063	-0.0738	-0.0737	-0.0738	0.0001	0.0000
0.9688	-0.0258	-0.0255	-0.0257	0.0002	0.0001

Error Estimate: We derive the absolute error of the Müntz – Legendre wavelet operational matrix method (MLWOMM). This technique allows comparing our findings to the exact solutions as well as numerical solutions obtained through other approaches of HWOMM. The absolute error is used to determine the precision of the suggested method. We use the definition

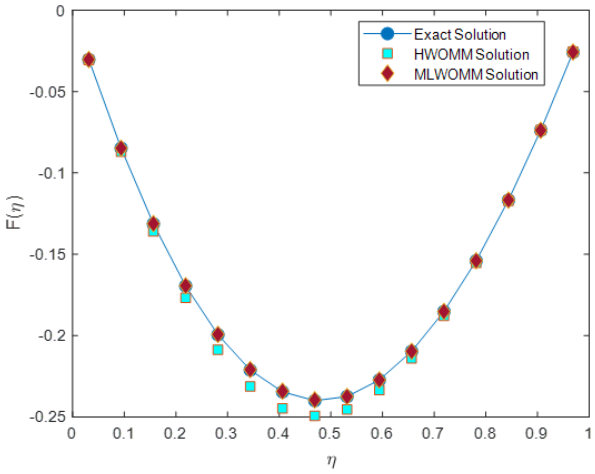

Fig 1. Numerical solution of the MLWOMM and HWOMM with the exact solutions of the test problem 1

of absolute error to compare the approximate solutions and exact solutions of the proposed method. The absolute error can be defined as[14],

$e(\eta) = |F(\eta) - F^*(\eta)|, \quad \eta \in [0,1).$

Here, $F(\eta) and F^*(\eta)$ are represented by exact solutions and approximated solutions of MLWOMM and HWOMM.

Heat transfer Problem 2. Lastly, we consider the thermal radiation problem in the heat transfer, we solve the third-order nonlinear thermal radiation problem on natural convection of vertical plate embedded in a saturated porous medium. This problem is solved by using the Müntz – Legendre wavelet operational matrix method.

The mathematical formulation of the problem : Let us consider the 2-dimensional viscous incompressible fluid flow induced by steady natural convection warmed vertical plate immersed in a saturated porous medium with the T_∞ outside temperature distribution. The viscous fluids are considered Newtonian, with the plate surface being subjected to continual fluid blowing or suction. The governing boundary equations for this problem can be expressed, and taking into Boussinesq and Darcy approximations can be introduced as[2,3] :

$$\frac{\partial u}{\partial x} + \frac{\partial v}{\partial y} = 0, \tag{29}$$

$$\frac{\partial u}{\partial y} = \frac{gK\beta}{v}\frac{\partial T}{\partial y}, \tag{30}$$

$$\left(u\frac{\partial T}{\partial x} + v\frac{\partial T}{\partial y}\right) = \frac{1}{\rho C_p}\left(k\frac{\partial^2 T}{\partial y^2} - \frac{\partial Q_r}{\partial y}\right). \tag{31}$$

The associated boundary conditions are:

$$\begin{aligned} &x \geq 0, \quad T(x,0) = T_w(x), \quad v(x,0) = V_w(x), \quad \text{at } y = 0 \\ &x \geq 0, \quad T(x,\infty) = T_\infty, \quad u(x,\infty) = 0, \quad \text{at } y = \infty\}, \end{aligned} \tag{32}$$

Here, u and $v$are represents velocities along x and $y$co-ordinates respectively, T is the viscous fluid temperature, C_p is the specific heat at constant pressure, ρ is the density of the fluid, k is the equivalent thermal diffusivity, v is the kinematic viscosity, K is the porous medium's permeability, β is the coefficient of thermal expansion and g is the gravitational acceleration. We assume that temperature distribution on the plate is governed by the power-law equation $T_w = T_\infty + Ax^\lambda$, Here, A is a non-negative

constant for heated plates, and λ is the temperature exponent. The radiation heat flux based on the Rosseland diffusion model for thermal radiation heat flux is expressed as[3] :

$$Q_r = -\frac{4\sigma}{3\chi}\frac{\partial T^4}{\partial y}\,. \tag{33}$$

Here, χ and σ are the Rosseland mean absorption constant and Stefan−Boltzmann coefficient. We assume that T^4 is a linear function temperature since temperature changes within the flow are negligible. As a result, T^4 is expanded in a Taylor series T_∞ while higher-order terms are ignored. The following term T^4can be represented as:

$$T^4 \approx 4TT_\infty^3 - 3T_\infty^4, \tag{34}$$

The system of partial differential equations is transformed into a simple nonlinear ordinary differential equation by using similarity transformations. We introduce and use the similarity transformations and parameters[2], we have:

$$\left.\begin{array}{lll} \Psi(x,y) = \alpha Ra_x F(\eta), & Ra_x = \dfrac{g\beta K(T_w - T_\infty)x}{\alpha v}, & T = T_\infty + Ax^\lambda \theta(\eta) \\ R_d = \dfrac{16\sigma T_\infty^3}{3\gamma k}, & \eta(x,y) = \dfrac{y}{x}Ra_x^{1/2}, & \theta(\eta) = \dfrac{T - T_\infty}{T_w - T_\infty}, \alpha = \dfrac{k}{\rho Cp} \end{array}\right\}, \tag{35}$$

Here, Ra_x is the modified Darcy-Rayleigh number, and the stream function $\Psi(x,y)$ is denoted as

$$v = -\frac{\partial \Psi}{\partial x} = -\left(\frac{\alpha}{2x}\right) Ra_x^{1/2}\left[(\lambda+1)F + (\lambda-1)F'\right], \quad u = \frac{\partial \Psi}{\partial y} = \frac{\alpha}{x} Ra_x F'(\eta). \tag{36}$$

And Eqns. (30) and (31) become the system of nonlinear ordinary differential equations with boundary conditions as the results follow:

$$F''(\eta) = \theta'(\eta), \tag{37}$$

$$\theta''(\eta) + \frac{\lambda+1}{2(R_d+1)}F(\eta)\theta'(\eta) - \frac{\lambda}{(R_d+1)}F'(\eta)\theta(\eta) = 0. \tag{38}$$

Here, the prime represents differentiation concerning η, λ represents temperature exponent, and R_d represents thermal radiation parameter. We see in Eq. (35), and the boundary conditions (32), are transformed into suitable boundary conditions, we have:

$$\left.\begin{array}{ll} F(0) = f_m, & F'(\infty) = 0, \\ \theta(0) = 1, & \theta(\infty) = 0, \end{array}\right\}. \tag{39}$$

The speed of injection or suction at the flat plate surface is given by:

$$v(x,0) = -\left(\frac{\alpha}{2x}\right) Ra_x^{1/2}(1+\lambda)F(0), \tag{40}$$

Here, $f_m = F(0)$ is the injection or suction parameter with the value of parameter $f_m > 0$ or $f_m < 0$. The fluid's entrainment velocity is given by;

$$v(x,\infty) = -\left(\frac{\alpha}{2x}\right) Ra_x^{1/2}(1+\lambda)F(\infty). \tag{41}$$

By inserting Eq. (37) into (38), we get the third-order nonlinear ordinary differential Eq. (42) connected with the boundary conditions in Eq. (43) we have:

$$F'''(\eta) + \frac{\lambda+1}{2(R_d+1)}F''(\eta)F(\eta) - \frac{\lambda}{(R_d+1)}\left(F'(\eta)\right)^2 = 0. \tag{42}$$

With corresponding boundary conditions are as follows:

$$F(0) = f_m, \quad F^{'}(0) = 1, \quad F^{'}(\infty) = 0. \tag{43}$$

We observe the Eqns. (37), (38), and (39) that $F'(\eta) = \theta(\eta)$ indicate the vertical velocity and temperature profiles are identical. The Rayleigh and Nusselt's local number can be represented as follows:

$$Nu_x Ra_x^{-1/2} = -\theta^{'}(0). \tag{44}$$

LWOMM solution of the heat transfer problem (42) with (43) is as follows: We developed a numerical solution for third-order nonlinear ordinary differential equations by using to solve MLWOMM, with a finite interval $[0,1)$. The problem Eq. (42) is a semi-infinite physical domain that is shortened to a finite domain by adding an unknown finite boundary η_∞, and the problem is normalized by introducing coordinate transformation [21] , In Eq. (43), the corresponding boundary condition of $F'(\infty) = 0$, let we take $\eta_\infty = 1$ that implies $F'(1) = 0$. The general method of solution we have already discussed in section 3. Here, we use the same procedure, Now we have substituted the values of $F(\eta), \quad F'(\eta), \quad F''(\eta), \quad F'''(\eta)$ and $F''(0)$ from section 2.2, in Eq. (42) with corresponding boundary conditions in Eq. (43) and applied them to collocation points in Eq. (12), and finally, a nonlinear system is obtained.

$$\begin{aligned} &a^T\Phi(\eta) + \frac{\lambda+1}{2(R_d+1)}\left\{\left(f_m + \eta + \frac{\eta^2}{2}\left(-1-a^TE\right) + a^TR(\eta)\right) \times \left(\left(-1-a^TE\right) + a^TP(\eta)\right)\right\} - \\ &\frac{\lambda}{(R_d+1)} \times \left[\left(1+\eta\left(-1-a^TE\right) + a^TQ(\eta)\right)\right]^2 = 0, \end{aligned} \tag{45}$$

here, $\Phi(\eta), \quad P(\eta), Q(\eta), R(\eta), E, l = 0,1,2,3,\ldots,2^{k-1} \times M$ are the $\left(2^{k-1} \times M\right) \times \left(2^{k-1} \times M\right)$ square matrices and E are the column matrix coefficients of Müntz – Legendre wavelet. Solving the nonlinear system Eq. (45) to find the unknown Müntz – Legendre wavelet coefficients $a_i's$ Newton's iterative technique is used. In this Newton's iterative approach to solving by using Matlab software 2020a, initially, we take the level of resolution values k and M, we have also taken collocation points, Next, the level of resolution k, M, increases the scale of matrices also increases. The main advantage of this algorithm's results is to decreases and it takes less time to compute and execute for the numerical solution of BVPs. And calculate the unknown coefficients of $a_i's$ are using Newton's iterative approach successfully applied. This technique is repeated until the required exactness is reached. The obtained results of the MLWOMM solutions are demonstrated in terms of tables and graphs. The effectiveness of MLWOMM is presented and comparison solutions are shown in Figure 2 and Table 2

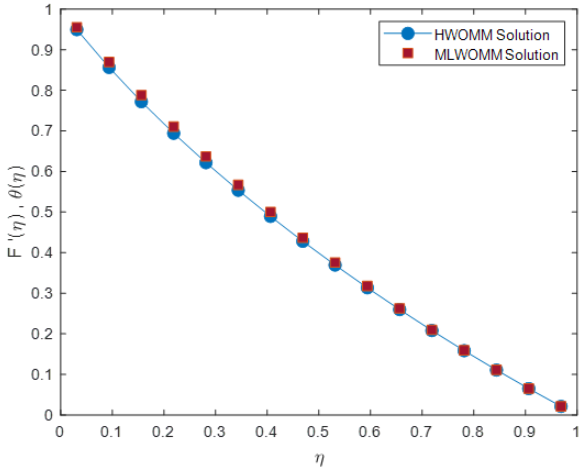

Fig 2. Numerical solutions of MLWOMM and HWOMM solutions at $f_m = 1$ of of the Heat transfer Problem 2.

3 Results and Discussion

The study presents that the computations were performed numerically to analyze the boundary value problem represented by Eq. (27) and the heat transfer problem (Eq. (42)) with corresponding boundary conditions provided by Eq. (43) on the semi-

Table 2. Comparison of MLWOMM results with the HWOMM results of the Heat transfer problem 2.

For instance $k = 2, M = 8$, at $\lambda = 1$, $R_d = 1$				
For $f_m = 1$			For $f_m = -1$	
η	**HWOMM Solution of** $F'(\eta), \theta(\eta)$	**MLWOMM Solution of** $F'(\eta), \theta(\eta)$	**HWOMM Solution of** $F'(\eta), \theta(\eta)$	**MLWOMM Solution of** $F'(\eta), \theta(\eta)$
0.0313	0.9495	0.9556	0.9689	0.9703
0.0938	0.8564	0.8703	0.9078	0.9110
0.1563	0.7720	0.7892	0.8475	0.8517
0.2188	0.6942	0.7122	0.7878	0.7921
0.2813	0.6217	0.6390	0.7283	0.7323
0.3438	0.5537	0.5693	0.6688	0.6722
0.4063	0.4893	0.5029	0.6090	0.6115
0.4688	0.4280	0.4397	0.5487	0.5503
0.5313	0.3695	0.3759	0.4878	0.4893
0.5938	0.3135	0.3180	0.4260	0.4269
0.6563	0.2598	0.2628	0.3633	0.3637
0.7188	0.2081	0.2100	0.2996	0.2997
0.7813	0.1585	0.1596	0.2349	0.2348
0.8438	0.1108	0.1114	0.1691	0.1690
0.9063	0.0651	0.0653	0.1023	0.1021
0.9688	0.0212	0.0213	0.0343	0.0343

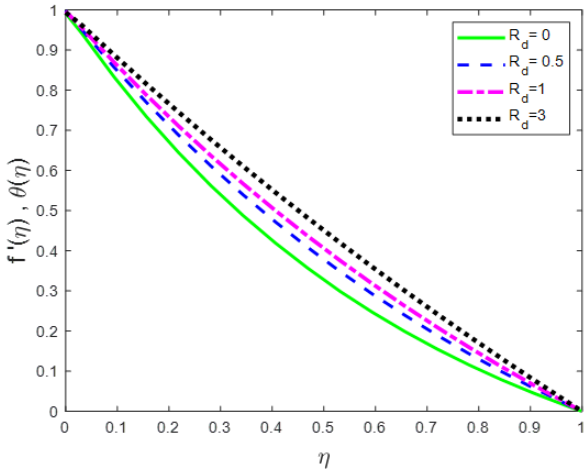

Fig 3. Vertical velocity or temperature profiles $\lambda = 1, f_m = 1$, for various values of R_d.

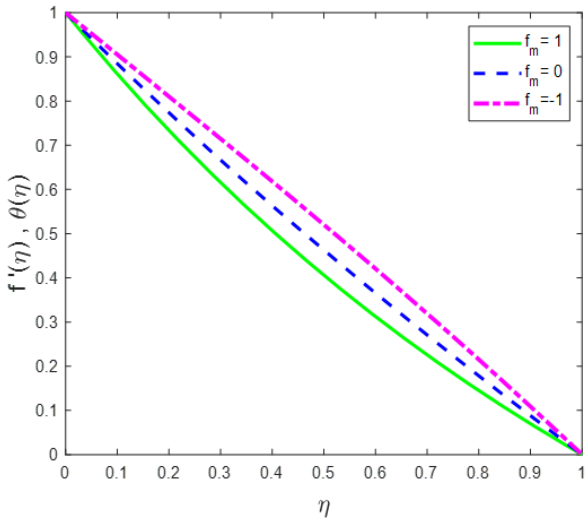

Fig 4. Velocity or Temperature profiles $\lambda = 1, R_d = 1$, for various values of f_m.

infinite domain is solved by using the MLWOMM as described in Section 2.2. First, we solved the test problem of the boundary value problem given in Eq. (27) with the exact solution, the purpose of solving this problem is to check the accuracy of our proposed method and confirms by verifying our MLWOMM results. The collected results are presented in terms of Tables and Graphs. The effectiveness of MLWOMM is presented by comparison with exact solutions and HWOMM solutions which are demonstrated in Table 1, and Figure 1 shows the numerical results of MLWOMM and HWOMM solutions. The display, Tables, and Graphs clearly show that the comparisons of MLWOMM solutions are in great agreement with the exact solutions, and more accurate solutions compare to HWOMM solutions. Next, we select the thermal radiation problem with Eq. (42), and Eq. (43) to be solved by using MLWOMM in Matlab software 2020a.

Table 2 and Figure 2 are displayed for the results of the heat transfer problem, the vertical velocity or temperature profile results of MLWOMM that found that they are more accurate compared to the HWOMM results. We observed these results in Table 2, For instance, $k = 2,\ M = 8,\ \lambda = 1,\quad R_d = 1$ when the suction/injection parameter $f_w = 1$, the velocity or temperature profile results are decreases compare to the suction/injection parameter $f_w = -1$. Displayed Figure 2, clearly shows the comparison of MLWOMM solutions is more accurate than the HWOMM solutions.

Displayed Figures 3 and 4 clearly show solutions for the temperature of the plate with constant lateral mass flux ($\lambda = 1$) controlled by the f_w with the R_d. The exponential decay temperature $\theta(\eta)$or velocity $F'(\eta)$ profiles through the boundary layers are confirmed in Figures 3 and 4. The calculations of suction/injection parameters f_m were performed for different cases, in the presence of thermal radiation R_d, which corresponds to the parameters are suction $f_m > 0$, injection $f_m < 0$, and impermeable plate $f_m = 0$. The velocity $F'(\eta)$ or temperature profiles $\theta(\eta)$ are numerical results illustrated in Figures 3 and 4, for the parameters λ, f_m and R_d be the selected values of the thermal radiation problem. In Figure 3 we observed that the fluid velocity or temperature profile rate increases with increasing values of the thermal radiation parameter R_d. This is because the effect of radiation R_d is to increase the rate of energy transport to the fluid, and therefore the fluid temperature. And also Figure 4 shows Suction greatly reduces the thickness of the boundary layer for $f_m = 1$, whereas injection significantly increases it for $f_m = -1$; however, the flow of heat surface is always non-negative, regardless of the value of f_m, because heat is transferred from the surface to the porous medium.

Overall we observe in the tables and graphs, that the numerical outcomes which are obtained by using MLWOMM are in very excellent agreement with the obtained HWOMM results. On the contrary, the typical Haar wavelet technique produces a good solution, but MLWOMM produces excellent solutions when it is compared with HWOMM solutions. As MLWOMM results are more accurate than HWOMM results. And also vertical velocity or temperature profile rate was studied.

4 Conclusion

In the present article, we studied the heat transfer of the thermal radiation effect on natural convection around a vertical flat surface immersed in a saturated porous medium. Initially, to ensure the efficiency of the proposed strategy, a third-order

nonlinear boundary value problem having the exact solution is presented as a test problem. Next, formulated Heat transfer problem, the governing equation of the problem with proper boundary conditions is reduced into the nonlinear ordinary differential equations by applied similarity transformations. The nonlinear problems with finite intervals are numerically solved by using MLWOMM. The effect of the thermal radiation parameters R_d, with the injection/suction of fluid f_m, and the temperature exponent's parameter λ are discussed graphically. And also the effect of fluid velocity or temperature profile rate was studied. Furthermore, the obtained MLWOMM results are in very excellent agreement with the obtained HWOMM results and the more accurate than HWOMM results.

5 Acknowledgement

The authors thank UGC-SAP DRS-III for 2016-2021:F.510/3/DRS-III / 2016(SAP-I) Dated: 29th Feb. 2016. And this work is supported by Karnatak University, Dharwad (KUD), Karnataka, India through a University Research Studentship (URS) during the year 2018-2021: KU.40 (SC/ST) sch/URS/2020-21/44/544, dated 12/12/2020.

References

1) Donald A, Nield A, Bejan A. Springer International Publishing. 2017. Available from: http://library.lol/main/2F8F5BDF933FC0BA87F849C58065BFBA.
2) Cortell R. Internal heat generation and radiation effects on a certain free convection flow. *International Journal of Nonlinear Science*. 2010;9(4):468–469. Available from: http://www.internonlinearscience.org/upload/papers/20110304105341181.pdf.
3) Achemlal D, Sriti ME, Haroui M, Guedda M. Free convection modeling over a vertical flat plate embedded in saturated porous medium with a variable heat source and radiation flux. *World Journal of Modelling and Simulation*. 2013;9(3):163–172. Available from: https://citeseerx.ist.psu.edu/viewdoc/download?doi=10.1.1.568.2669&rep=rep1&type=pdf.
4) Anwar T, Kumam P, Shah Z, Watthayu W, Thounthong P. Unsteady Radiative Natural Convective MHD Nanofluid Flow Past a Porous Moving Vertical Plate with Heat Source/Sink. *Molecules*. 2020;25(4):854. Available from: https://doi.org/10.3390/molecules25040854.
5) Nourhan I, Ghoneim MG, Reddy AM, Megahed. Numerical solution for natural convection fluid flow along a vertical cone with variable diffusivity and wall heat and mass fluxes embedded in a porous medium. *International Journal of Modern Physics C*;2021(6):2150074. Available from: https://doi.org/10.1142/S0129183121500741.
6) Mahdy A, El-Zahar ER, Rashad AM, Saad W, Al-Juaydi HS. The Magneto-Natural Convection Flow of a Micropolar Hybrid Nanofluid over a Vertical Plate Saturated in a Porous Medium. *Fluids*. 2021;6(6):202–202. Available from: https://doi.org/10.3390/fluids6060202.
7) Jha BK, Samaila G. Numerical solution for natural convection flow near a vertical porous plate having convective boundary condition with nonlinear thermal radiation. *Heat Transfer*. 2022;51(2):1711–1724. Available from: https://doi.org/10.1002/htj.22371.
8) Jha BK, Samaila G. Nonlinear Approximation for Natural Convection Flow Near a Vertical Plate With Thermal Radiation Effect. *Journal of Heat Transfer*. 2021;143(7):74501. Available from: https://doi.org/10.1115/1.4050854.
9) Roja P, Reddy T, Ibrahim SM, Lorenzini G. Nor Azwadi Che Sidik. The Effect of Thermophoresis on MHD Stream of a Micropolar Liquid through a Porous Medium with Variable Heat and Mass Flux and Thermal Radiation. *CFD Letters*. 2022;14(5):106–124. Available from: https://doi.org/10.37934/cfdl.14.5.106124.
10) Jha BK, Samaila G. Impact of nonlinear thermal radiation on nonlinear mixed convection flow near a vertical porous plate with convective boundary condition. *Proceedings of the Institution of Mechanical Engineers, Part E: Journal of Process Mechanical Engineering*. 2022;236(2). Available from: https://doi.org/10.1177/09544089211064386.
11) Alqarni MM, Amin R, Shah K, Nazir S, Awais M, Alshehri NA, et al. Solution of third order linear and nonlinear boundary value problems of integro-differential equations using Haar wavelet method. *Results in Physics*. 2021;25:104176. Available from: https://doi.org/10.1016/j.rinp.2021.104176.
12) Shiralashetti SC, Harishkumar E. Haar wavelet matrices for the numerical solution of a system of ordinary differential equations. *Malaya Journal of Matematik*. 2020;1:144–147. Available from: https://doi.org/10.26637/MJM0S20/0027.
13) Shiralashetti SC, Hanaji SI, Naregal SS. Daubechies wavelet based numerical method for the solution of grease elastohydrodynamic lubrication problem. *AIP Conference Proceedings*. 2020;2246:20029. Available from: https://doi.org/10.1063/5.0014591.
14) Shiralashetti SC, Lamani L. Fibonacci wavelet based numerical method for the solution of nonlinear Stratonovich Volterra integral equations. *Scientific African*. 2020;10:e00594. Available from: https://doi.org/10.1016/j.sciaf.2020.e00594.
15) Shiralashetti SC, Badiger P. Chebyshev wavelets approach for the squeeze film lubrication of long porous journal bearings with couple stress fluids. *Malaya Journal of Matematik*. 2020;1:138–143. Available from: https://doi.org/10.26637/MJM0S20/0026.
16) Shiralashetti SC, Hanaji SI. Hermite wavelet based numerical method for the solution of two parameters singularly perturbed non-linear Benjamina-Bona-Mohany equation. *Scientific African*. 2021;12:e00770. Available from: https://doi.org/10.1016/j.sciaf.2021.e00770.
17) Shiralashetti SC, Deshi AB. Numerical solution of differential equations arising in fluid dynamics using Legendre wavelet collocation method. *International Journal of Computational Materials Science and Engineering*. 2017;06(02):1750014. Available from: https://doi.org/10.1142/S2047684117500142.
18) Daubechies I. *Ten Lectures on Wavelets, Society for Industrial and Applied Mathematics*. 1992. Available from: https://epubs.siam.org/doi/pdf/10.1137/1.9781611970104.fm.
19) Shiralashetti SC, Hanaji SI, Naregal SS. Haar wavelet based numerical method for the solution of non-linear partial differential equation. *AIP Conference Proceedings*. 2020;2246:20033. Available from: https://doi.org/10.1063/5.0014599.
20) Shiralashetti SC, Kumbinarasaiah S. New generalized operational matrix of integration to solve nonlinear singular boundary value problems using Hermite wavelets. *Arab Journal of Basic and Applied Sciences*. 2019;26(1):385–396. Available from: https://doi.org/10.1080/25765299.2019.1646090.
21) Karkera H, Katagi NN. Wavelet-Based Numerical Solution for MHD Boundary-Layer Flow Due to Stretching Sheet. *International Journal of Applied Mechanics and Engineering*. 2021;26(3):84–103. Available from: https://doi.org/10.2478/ijame-2021-0037.
22) Awati VB, Kumar NM. Analysis of Forced Convection Boundary Layer Flow and Heat Transfer Past a Semi-Infinite Static and Moving Flat Plate Using Nanofluids-by Haar Wavelets. *Journal of Nanofluids*. 2021;10(1):106–117. Available from: https://doi.org/10.1166/jon.2021.1771.

23) Rahimkhani P, Ordokhani Y. Application of Müntz–Legendre polynomials for solving the Bagley–Torvik equation in a large interval. *SeMA Journal*. 2018;75(3):517–533. Available from: https://doi.org/10.1007/s40324-018-0148-2.
24) Rayal A, Verma SR. Numerical study of variational problems of moving or fixed boundary conditions by Muntz wavelets. *Journal of Vibration and Control*. 2022;28(1-2):214–229. Available from: https://doi.org/10.1177/1077546320974792.
25) Rahimkhani P, Ordokhani Y, Babolian E. Müntz-Legendre wavelet operational matrix of fractional-order integration and its applications for solving the fractional pantograph differential equations. *Numerical Algorithms*. 2018;77(4):1283–1305. Available from: https://doi.org/10.1007/s11075-017-0363-4.
26) Dang QA, Dang QL. Simple numerical methods of second- and third-order convergence for solving a fully third-order nonlinear boundary value problem. *Numerical Algorithms*. 2021;87(4):1479–1499. Available from: https://doi.org/10.1007/s11075-020-01016-2.